Article

Cell Reports

Reliable and Elastic Propagation of Cortical Seizures In Vivo

Graphical Abstract

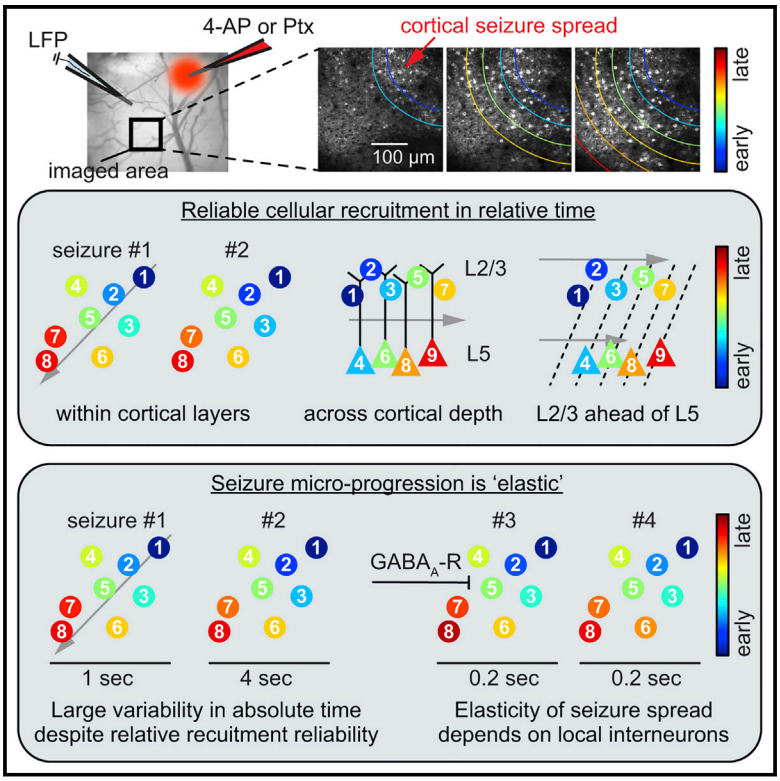

Highlights

- Seizures spread reliably through cortical microcircuits, within and across layers
- Seizures recruit supra-granular layers ahead of deep layers
- Despite relative reliability, recruitment is variable in absolute time (elasticity)
- Elasticity of ictal progression is shaped by local GABAergic interneurons

Authors

Michael Wenzel, Jordan P. Hamm, Darcy S. Peterka, Rafael Yuste

Correspondence

mw2946@columbia.edu

In Brief

Wenzel et al. map cortical seizure spread at cellular resolution in vivo, and they show that seizures spread reliably, with repeated cell-wise and layer-wise recruitment patterns, yet with greatly variable recruitment durations in absolute time. This elasticity is controlled by inhibitory interneurons, as local GABAA-R blockade abolishes the phenomenon.

Wenzel et al., 2017, Cell Reports *19*, 2681–2693
June 27, 2017
http://dx.doi.org/10.1016/j.celrep.2017.05.090

Cell Reports
Article

Reliable and Elastic Propagation of Cortical Seizures In Vivo

Michael Wenzel,[1,2,*] Jordan P. Hamm,[1] Darcy S. Peterka,[1] and Rafael Yuste[1]
[1]Neurotechnology Center, Department of Biological Sciences, Columbia University, New York, NY 10027, USA
[2]Lead Contact
*Correspondence: mw2946@columbia.edu
http://dx.doi.org/10.1016/j.celrep.2017.05.090

SUMMARY

Mapping the fine-scale neural activity that underlies epilepsy is key to identifying potential control targets of this frequently intractable disease. Yet, the detailed in vivo dynamics of seizure progression in cortical microcircuits remain poorly understood. We combine fast (30-Hz) two-photon calcium imaging with local field potential (LFP) recordings to map, cell by cell, the spread of locally induced (4-AP or picrotoxin) seizures in anesthetized and awake mice. Using single-layer and microprism-assisted multilayer imaging in different cortical areas, we uncover reliable recruitment of local neural populations within and across cortical layers, and we find layer-specific temporal delays, suggesting an initial supra-granular invasion followed by deep-layer recruitment during lateral seizure spread. Intriguingly, despite consistent progression pathways, successive seizures show pronounced temporal variability that critically depends on GABAergic inhibition. We propose an epilepsy circuit model resembling an elastic meshwork, wherein ictal progression faithfully follows preexistent pathways but varies flexibly in time, depending on the local inhibitory restraint.

INTRODUCTION

Epilepsy represents a wide range of pathological neural network alterations characterized by recurrent episodes of excessive brain activity. Identifying properties of seizure-producing networks (ictal networks) may enable more efficient seizure control (Baraban and Löscher, 2014; Krook-Magnuson and Soltesz, 2015). Recent advances in mapping ictal network dynamics at the microscale have unveiled unexpected complexity (Bower et al., 2012; Cymerblit-Sabba and Schiller, 2012; Feldt Muldoon et al., 2013; Keller et al., 2010; Truccolo et al., 2011, 2014), challenging the classical view of epilepsy as a condition of stereotyped ictal events (Szabo et al., 2015). In fact, the monitoring of the recruitment of neural populations to successive seizures in humans using multi-electrode arrays has led to contrasting conclusions, suggesting strict reproducibility of neuronal spiking patterns (Truccolo et al., 2011), a lack of such reproducibility close to the epileptic focus (ictal penumbra or propagation area) (Schevon et al., 2012), or completely non-repeated recruitment patterns (Bower et al., 2012). Part of the reason behind this controversy could be technical: it remains challenging for multi-electrode approaches to disambiguate the activity of densely packed neuronal circuits, especially for cells far from the electrode. Electrical recordings are inherently sparse when compared to the actual neural population density, complicating definitive conclusions. On the other hand, the few in vitro reports employing high-resolution optical imaging of ictal networks had too low a temporal resolution to uncover the true spatiotemporal dynamics of ictal networks (Badea et al., 2001; Cammarota et al., 2013; Feldt Muldoon et al., 2013; Lillis et al., 2015; Neubauer et al., 2014; Tashiro et al., 2002; Trevelyan et al., 2007).

To date, there have been only two studies using optical methods to measure the recruitment of epileptic networks at a cellular scale in vivo (Baird-Daniel et al., 2017; Muldoon et al., 2015). Baird-Daniel et al. (2017) compared the differential recruitment of glial versus neuronal populations to acute seizures at a population scale. Muldoon and colleagues (Muldoon et al., 2015) did not map seizures but interictal spikes, and they demonstrated heterogeneous recruitment of local microcircuits across seemingly stereotyped local field potential (LFP) events. Thus, despite being of great conceptual and therapeutic interest, the recruitment dynamics of densely packed neural networks during cortical seizure progression have still not been characterized in detail. In addition, it is unknown if there are layer-specific recruitment dynamics during ictal spread in vivo. However, understanding how exactly seizures progress in the living brain may hold critical new clues on how to stop their expansion.

To address these questions, we combined fast 30-Hz resonant two-photon calcium imaging with LFP recordings in two mouse models of acute seizures (4-Aminopyridine [4-AP] or picrotoxin [Ptx]) in anesthetized and awake mice, imaging both supra- and infragranular layers in different cortical areas. We find that neural recruitment to ictal activity maintains relative spatiotemporal reliability, even at the single-cell level, and that this reliability holds true across cortical areas and layers, with an initial supra-granular cortical invasion closely followed by recruitment of deep layers. However, absolute temporal micro-progression of seizures varies profoundly across events, revealing a constrained ictal network that flexibly stretches and

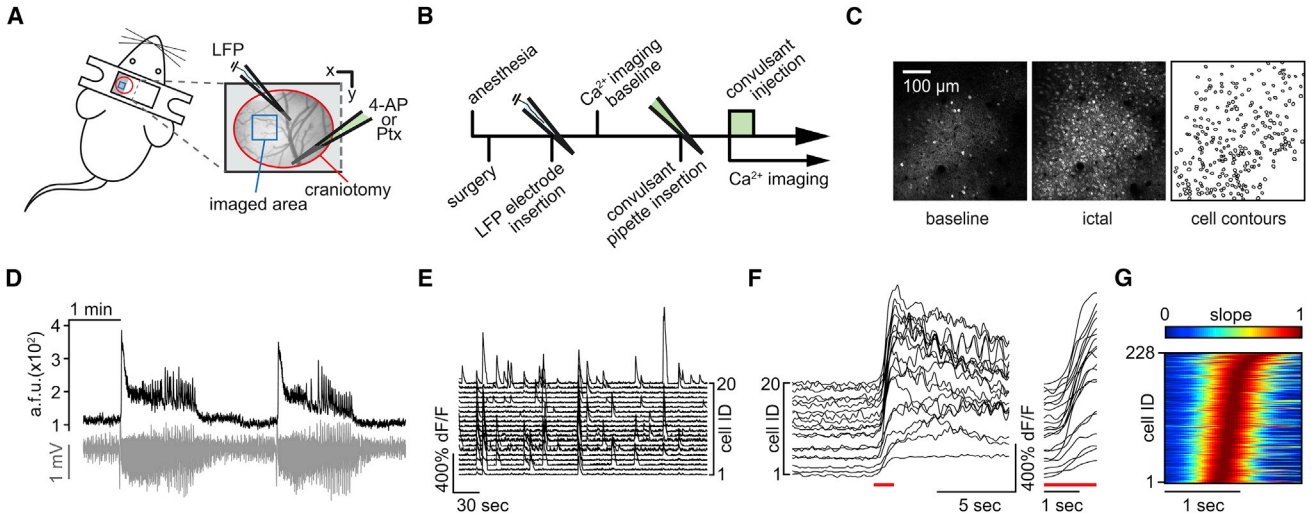

Figure 1. In Vivo Two-Photon Calcium Imaging of Seizure Spread with Single-Cell Resolution

(A) Experimental setup with surgical approach over left somatosensory cortex (craniotomy encircled in red and imaged field of view (FOV) within the seizure propagation area in blue). Each experiment (exp.) involved the insertion of two glass micropipettes, one (blue) containing a silver chloride electrode for local field potential (LFP) recording and the other (green) containing 4-AP (15 mM, injection vol. 500 nL [total amount delivered = 7.5 nmol]) or Ptx (10 mM, injection vol. 500 nL [total amount delivered = 5 nmol]).

(B) Typical experimental workflow.

(C) Propagation area in left somatosensory cortex, representative 3-s average (avg) fluorescence images of neural activity (GCaMP6s) during baseline (left) and full ictal event (middle, see also Movie S1). Contour plot of registered cells (right) is shown.

(D) Average calcium transient of FOV (black trace, GCaMP6s, imaging depth ~150 μm beneath the pial surface) and corresponding LFP (gray trace) post 4-AP.

(E) Calcium transients of 20 representative cells within FOV during baseline.

(F) The same 20 cells post 4-AP, with optical seizure break-in (underlined in red) magnified on the right.

(G) Representative example of the optical break-in of the ictal wave (normalized first derivative of ΔF/F). Cell recruitment to ictal activity was ordered in time by maximum slope.

compresses in time. We show that this progression elasticity (i.e., relative spatiotemporal reliability despite progression variability in absolute time) critically hinges on the activity of local GABAergic interneurons, as compromising their signaling results in the acceleration and invariance of ictal progression. Thus, cortical circuits, at least during seizures, can propagate activity through the same pathways with greatly variable speeds and delays, both of which depend on the strength of the local inhibitory restraint to excessive network activity.

RESULTS

To map seizure propagation, we employed two pharmacological models of acute seizures using local cortical injection of small amounts of either 4-AP (15 mM, 500 nL [total amount delivered = 7.5 nmol], layer V) or Ptx (10 mM, 500 nL [total amount delivered = 5 nmol], layer V) in mature mouse neocortex. The two drugs generate seizures through different mechanisms. While the potassium channel blocker 4-AP enhances neuronal firing through increased pre-synaptic glutamate release (Morales-Villagrán and Tapia, 1996), the disinhibitory compound Ptx acts as GABA-A receptor antagonist (Krishek et al., 1996). The models provided a two-pronged approach for studying the repeated and variant spatiotemporal details of spreading seizures at a fine scale, in a setting where intra- and extrafocal compartments are precisely defined.

Two-Photon Calcium Imaging of Neocortical Seizure Spread In Vivo

We were interested in mapping cellular recruitment during spread of ictal activity, and we used in vivo two-photon calcium imaging (OGB-1, GCaMP6s, or GCaMP6f) to monitor action potential activity in neural populations (Chen et al., 2013; Stosiek et al., 2003; Yuste and Denk, 1995; Yuste and Katz, 1991). For imaging seizure spread during mild anesthesia, a small craniotomy above the somatosensory cortex was established (Figure 1A). As a gross indicator of ictal activity within the examined area, we measured the LFP with a sharp glass microelectrode, carefully lowered into the cortex next to the imaged field of view (FOV; Figure 1A). The positioning of the LFP pipette in proximity, yet outside the seizure initiation site, did not affect the temporal signature of electrographic seizures, even though LFP signal amplitude decreased with distance to the initiation site (Figure S1A). For the induction of ictal events, a second glass micropipette containing 4-AP was inserted into the cortex to a depth of ~480 μm after baseline imaging, at a distance of ~1.5–2 mm to the FOV (Figures 1A and 1B). No epileptiform activity was induced by saline injection alone (Figure S1B).

Animals' heart rate, breath rate, and peripheral blood oxygenation were monitored via a paw sensor throughout experiments to ensure stable vital parameters (Figure S1C). Even though leading to hundreds of interictal LFP spikes (IISs), Ptx injections did not lead to full ictal events during anesthesia (data not

shown), and they were henceforth used only in experiments during wakefulness. In the absence of any chemoconvulsant, local populations in layer II/III (LII/III) displayed ongoing sparse and distributed calcium activity during baseline (Figures 1C, left and 1E). In contrast, full ictal events post 4-AP entailed sustained firing of large numbers of neurons in the FOV (Figures 1C, middle, 1D, and 1F; Figure S1D; Movies S1 and S2). Ictal invasion happened in a continuous wave of intense neuronal firing that slowly propagated across the FOV. During anesthesia, 4-AP-induced electrographic seizures and imaged calcium transients corresponded in time (Figure 1D; Figure S1D), and the rise in calcium was correlated with the typical increase in spectral power of the ictal LFP signal over a wide frequency range (1–100 Hz), reflecting massive synaptic barrages during seizures (Figure S1E). However, individual calcium deflections could only be directly related to lower frequency ictal activity toward the end of seizures (see, e.g., Movie S2), because even fast calcium indicators like OGB-1 or GCaMP6f have too low temporal kinetics to resolve individual LFP deflections during tonic ictal firing (Khoshkhoo et al., 2017). The propagation velocity of the optical invasion of the FOV was similar to the Jacksonian march described in humans and experimental seizure models where inhibition is intact (seven experiments [exp.] under anesthesia, 71 seizures, 0.64 ± 0.18 mm/s) (Jasper, 1969; Trevelyan et al., 2007; Wong and Prince, 1990). Notably, the pre-ictal neural activity in not yet invaded areas during pending seizure spread was sparse, until the sharp rise in fluorescence upon arrival of the ictal wave front (Figures 1D and 1F; Figure S1D). This activity pattern was in sharp contrast to the seizure initiation site, where locally confined, enhanced calcium activity could be imaged almost immediately after 4-AP injection (data not shown). Importantly, our temporal imaging resolution of 30 Hz was sufficient to capture individual cell recruitment to ictal activity (Figures 1F and 1G; Figure S1D).

Stereotypical Spatiotemporal Recruitment of Neural Populations by Seizures

To investigate the characteristics of local network recruitment during seizure spread, we analyzed all neurons in the FOV that showed a visible change in fluorescence upon optical break-in of ictal activity and whose somata could be followed stably across the analyzed time period (n = 7 exp. under anesthesia [OGB-1 = 4, GCaMP6s = 3], total number of seizures = 71, average number of analyzed cells = 201 ± 25 SEM). Corresponding in time to the incoming ictal wave, neurons were recruited in a continuous, sigmoid temporal curve (Figure 2A). First, we mapped temporal population recruitment patterns, specifically examining the regularity of individual cell and sub-region recruitment to seizures. Arranging cell recruitment time points (maximum slope of ΔF/F) of an individual seizure revealed that the tilt of the temporal ordering was coarsely preserved across ictal events (Figure 2B). When we tiled the imaged region instead of registering individual cells (Figure S2A), this inherent temporal structure became apparent even in unsorted data (Figure S2B).

To quantify and verify this conserved structure at the single-cell scale, we used two different analytical approaches. First, regardless of its duration, we divided every ictal break-in into three equally sized time bins (early, intermediate, and late; Figure S2C, upper panel), calculating an SD of bin membership for each cell across the entire experiment such that, if a given cell were always recruited to the seizure at the same relative time, its SD would equal zero. We additionally established a more continuous method by classifying a cell's recruitment time relative to the entire population (similar to a *Z* score), separately for each seizure (relative recruitment score [rr score]; Figure S2C, lower panel). The observed time bin or rr score distributions for each cell and their SD were compared to randomized surrogate distributions derived from a temporal reshuffling procedure (Figure S2D). Both methods revealed left-shifted SD distributions, indicating a smaller relative onset time variability in the observed dataset than would be expected by chance given population recruitment (Figure 2C). To exclude the possibility that these results were biased by the cells' indicator load (e.g., the higher the load the sooner the measured recruitment), we performed a correlation analysis between cellular baseline fluorescence and the corresponding recruitment, which showed no systematic relationship (Figure 2D; all 4 OGB-1 exp., 42 seizures, 952 cells, $r = 0.1386$, $r^2 = 0.0192$; the effect accounts for 1.9% of the variance in the data).

After obtaining cellular time bin and rr score SDs, we generated a reliability index for individual cells that were defined as reliable when their SD was smaller than 95% ($p < 0.05$) of those in the randomized dataset. Again, both approaches revealed a substantial percentage of temporally reliably recruited neurons (Figure 2E, cells). This reliability further increased with growing spatial coarseness (Figure 2E, tiles). It is noteworthy that reliability indices of time binning and rr score classification were not necessarily built of the same cells but in fact had non-overlapping sections. The combined reliability index, where a cell was called reliable if reliable in at least one of the two methods (time bin or rr score), was higher than in either individual classification (Figure 2E, right).

The fact that cell and tile analyses showed stable relative recruitment ordering to subsequent seizures implied that seizures propagate in a spatially organized manner, and, indeed, we found a coarsely maintained spatial pattern of cell recruitment (Figure 2F). To quantify this effect, we implemented a two-dimensional ANOVA approach by categorizing cells based only on their recruitment times (i.e., temporal quartiles). We compared (1) the distance of individual cells to the spatial mean of their respective quartile to (2) the distance of all cells to the spatial mean of the entire analyzed population (Figure 2G, same experiment as in Figure 2F; Figure S2E). This approach yielded significant bivariate F values for all seven experiments (F values: $F[3,48] = 11.595$, $F[3,28] = 33.260$, $F[3,36] = 11.251$, $F[3,52] = 22.208$, $F[3,36] = 12.67$, $F[3,60] = 11.64$, and $F[3,8] = 41.224$; all p values < 0.001).

Stereotypical Local Population Recruitment Patterns across Cortical Layers

To test whether network reliability holds true across cortical layers, we employed a recently introduced technique enabling multilayer imaging through implanted glass microprisms (1 × 1 × 1 mm; Figure 3A) (Andermann et al., 2013). Again, a sharp glass microelectrode was carefully lowered into the cortex close by the prism face for LFP recordings (Figure 3A), and a second

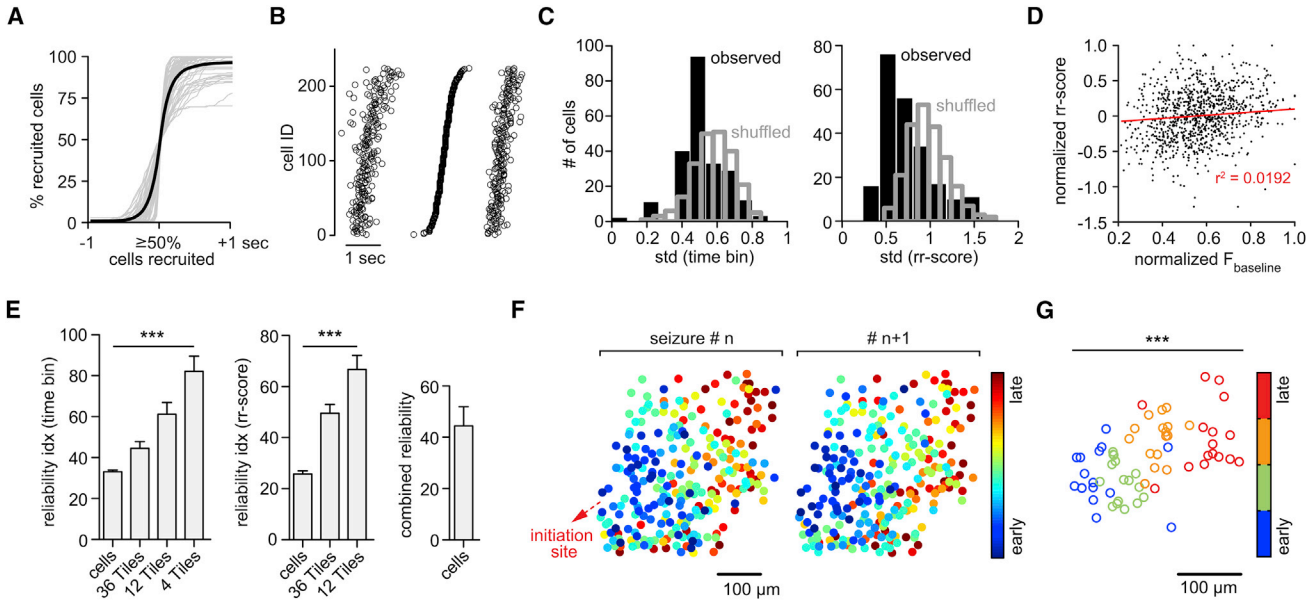

Figure 2. Stereotypical Micro-progression of Seizures

(A) Superposition of all analyzed optical seizure break-ins (gray) centered around the 50% recruitment frame. The black graph represents mean temporal recruitment (n = 7 exp., total number of seizures = 71 [11.3 ± 1.358 SEM], total number of cells analyzed = 1,402 [201 ± 25 SEM], cell number in percentage for comparability across experiments).

(B) Representative example of three consecutive optical seizure break-ins plotted next to each other. The first and third events are sorted by the temporal ordering of the second event. Each circle represents an individual cell recruitment time point.

(C) Representative experiment with observed (black) versus shuffled (gray) time bin or rr score SD distributions.

(D) Correlogram of cellular baseline fluorescence versus rr scores. Values are maximum-normalized for comparability across experiments. The relationship between the two parameters is negligible (four exp., 42 seizures, 952 cells, r = 0.1386, r^2 = 0.0192). The effect accounts for 1.9% of the variance in the data.

(E) Reliability indices displaying the percentage of cells or spatial sub-regions (tiles) whose temporal recruitment variability (time bin or rr score SD) are <5% of all shuffled values of analyzed cells or tiles ($p < 0.05$). Recruitment reliability increased with spatial coarseness (one-way ANOVA, n = 7 exp., total number of cells = 1,402; time bin and rr score classification, $p < 0.0001$). Right: combined (reliable in time bin and/or rr score classification) cell-wise reliability index is shown.

(F) Spatiotemporal maps of cell recruitment in two consecutive seizures indicating grossly preserved relative recruitment. Each dot represents an individual cell. 4-AP injection site (red arrow) is located ~1.5 mm posterior to FOV (somatosensory cortex).

(G) Same experiment. The spatial average coordinates of temporally defined population quartiles (25% earliest recruited cells, 25%–50%, 50%–75%, and 75%–100%) across 16 seizures show consistent spatiotemporal propagation (bivariate ANOVA: n = 16 seizures, F[3,60] = 11.64, p = 0.000004, all seven axial exp. under anesthesia, $p < 0.001$). Each circle represents the average coordinate of all cells belonging to the respective quartile.

sharp glass micropipette containing 4-AP was advanced into the cortex to a depth of ~480 μm, at a distance of ~1.5–2 mm to the implanted prism. Imaging was carried out at a distance of 180–300 μm from the vertical prism face, where no damage of the cortex was to be expected due to prism insertion (Chia and Levene, 2009b).

In accordance with previous reports (Andermann et al., 2013; Chia and Levene, 2009b), visualized vasculature and cell anatomy appeared physiological and local network activity showed sparse cell firing (Figure 3B; Movie S3), as observed during axial imaging of superficial layers (LII/III) during baseline. Correct vertical positioning of the prism was ensured by visualizing the full extent of layer V (LV) pyramidal neurons with their apical dendrites extending across layer IV (LIV) into LII/III. As observed in axial plane LII/III experiments, seizures invaded the imaged translaminar FOV in a continuous fashion (Figure S3B; Movies S4 and S5). Side-by-side plotting of individual cells' recruitment time points of consecutive seizures showed that the earlier observed coarse preservation of temporal recruitment within LII/III holds true across cortical depth (Figure 3C). Likewise, quantification of multilayer cell recruitment during lateral seizure spread revealed left-shifted SD distributions of individual cell bin memberships or rr scores (Figure 3D). Consequently, a substantial percentage of neurons in LII/III and LV was shown to occupy reliable relative temporal recruitment positions across seizures (Figure 3E). Again, spatiotemporal onset maps of successive seizures showed a maintained spatial pattern of relative cell recruitment (Figures 3F and 3G). These experiments showed that network recruitment reliability can be found across the cortical column.

Spreading Ictal Activity Recruits Superficial Cortex ahead of Deep Cortical Layers

During multilayer imaging, we noticed that relative temporal recruitment of local cell populations seemed to differ across layers (Figure 3G). To quantify layer-specific spatiotemporal recruitment delays, we located groups of neighboring neurons within spatial bins (or tiles) of 100-μm width in LII/III and LV, and we derived an average calcium population transient for every tile, for each electrographic seizure onset of an experiment

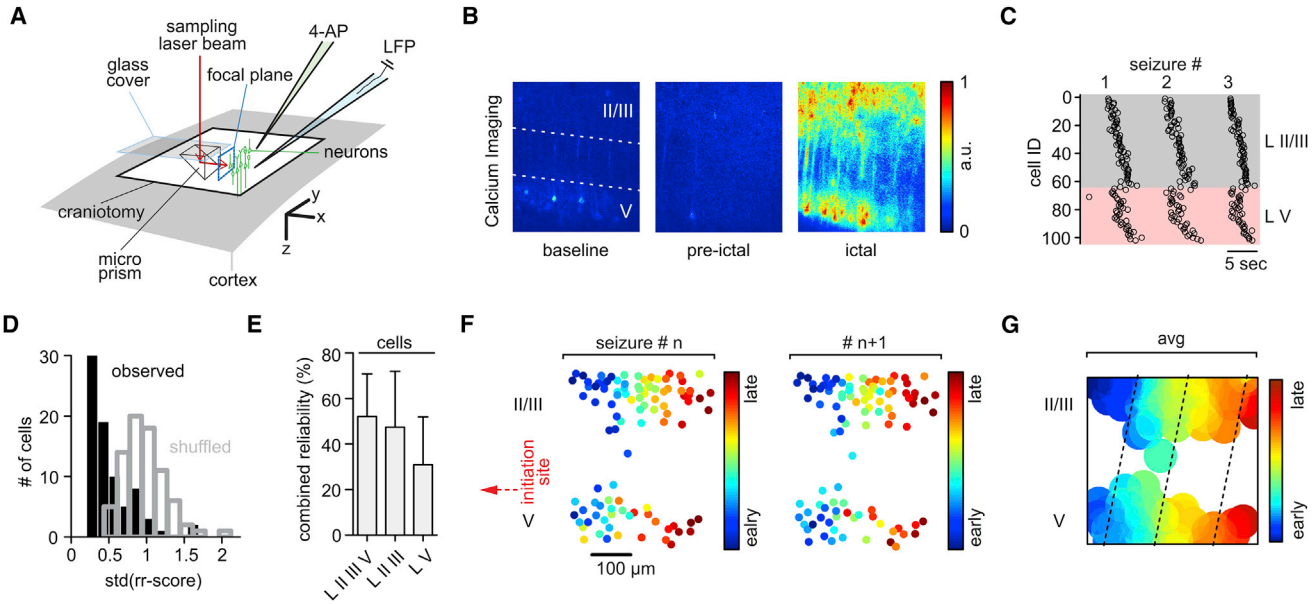

Figure 3. Stereotypical Seizure Propagation across Cortical Layers

(A) Experimental setup involving cortical microprism implant (brain surface in gray and craniotomy encircled in black). The 90-degree laser beam (red) deflection results in a vertical FOV (neurons in green); again, each experiment involved the insertion of two glass pipettes (LFP, blue and 4-AP, green).

(B) Representative 3-s average fluorescence images of multilayer neural activity, recorded under anesthesia in somatosensory cortex during baseline (left, II/III or V = layer II/III or V), directly prior to the seizure break-in (middle) and full ictal event (right, see also Movies S3, S4, and S5). The injection site of 4-AP was located ~2 mm anterolateral to the prism (in LV), aligned to the edge of the prism face.

(C) Representative example of three consecutive optical seizure break-ins plotted next to each other, indicating consistent recruitment across cortical layers. Each circle represents an individual cell recruitment time point.

(D) Representative experiment, observed (black) versus shuffled (blue) rr score SD distribution.

(E) Combined reliability index displaying the percentage of cells whose recruitment SD are <5% of all shuffled SD of all analyzed cells ($p < 0.05$, n = 4 exp., total number of seizures = 32 [8 ± 3.6 SEM], total number of cells analyzed = 334 [84 ± 13 SEM]).

(F) Spatiotemporal maps of multilayer cell recruitment in two consecutive seizures, indicating preserved cell recruitment. 4-AP injection site (red arrow) is located ~1.5 mm away from FOV.

(G) Same experiment, average contour plot of eight seizures. Note how LII/III appears to be recruited ahead of corresponding LV (dotted lines).

(Figure 4A; Figures S3C and S3D). In accordance with our results from axial imaging in LII/III (Figures 2F and 2G), tiles in LII/III being located more proximally to the seizure initiation site were consistently recruited earlier than those being situated more distant to it (Figure 4A; Figure S3C, blue traces). The same spatiotemporal pattern of progression was observed in LV (Figure 4A; Figure S3C, green traces). To our surprise, and in contrast to previous reports in disinhibited brain slices where LV led lateral spread of epileptiform activity (Telfeian and Connors, 1998), we observed an ictal recruitment of LII/III ahead of LV (Figure 4A; Figure S3). In fact, this bi-directional progression delay was already apparent to the naked eye when inspecting the raw data (Movies S4 and S5). To compare layer-specific delays across experiments, we calculated the recruitment time lags of adjacent tile pairs (lateral pairs: tile[prox] − tile[dist]; vertical pairs: tile[II/III] − tile[V]) for every seizure break-in (Figure S3D). In doing so, we did not only find significant layer-specific average negative time lags of proximal versus distal tiles in nearly all seizures but also proved a temporally variable yet consistent delay of local LV populations to their LII/III tile counterparts (Figures 4B and 4C). In sum, we found that cortical seizure spread in the intact brain involves lateral expansion within superficial and deep layers. Intriguingly, we reveal a vertical delay during lateral seizure spread, with a lead of LII/III recruitment over LV.

Mapping Cortical Seizure Micro-progression in Awake Mice

Major advancements in epilepsy research have been achieved by measurements in anesthetized animals. Yet, inherently, anesthesia alters neuronal network activity, and it does so in a non-uniform way (Adesnik et al., 2012). Therefore, we set out to investigate whether our findings hold true in the awake condition, using either local 4-AP or Ptx injection. Again, we recorded calcium activity and LFP in head-restrained yet otherwise freely moving mice, positioned on a running wheel that can tilt flexibly and therefore serve as a suspension during seizure-related motor symptoms. To maximize focal plane imaging stability in the awake state, a thin glass coverslip was positioned over the craniotomy, with a small opening established posterior to it for access of both the LFP and 4-AP or Ptx pipettes (Figure 5A).

Prior to the actual experiment, all animals were habituated to the experimenter and the experimental environment. Like in anesthetized mice, a series of full electrographic but now also behaviorally detectable seizures, including orofacial and

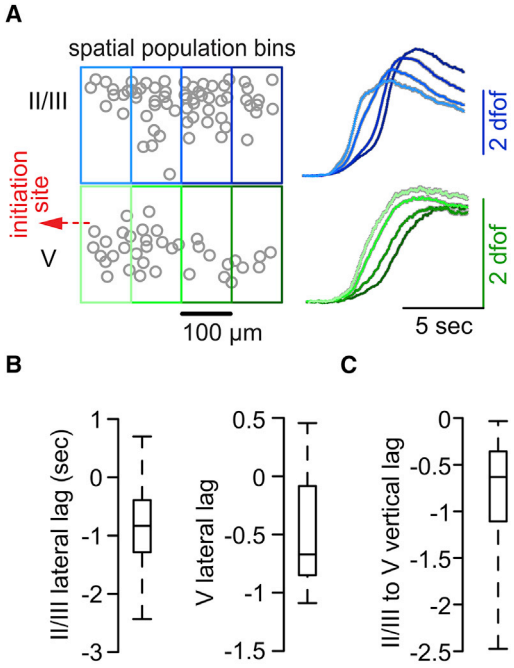

Figure 4. Supra-granular Layers Are Systematically Recruited ahead of Deep Layers

(A) Left: paradigmatic multilayer contour plot (LII/III and LV, circles represent individual cells). Small local cell populations were grouped together in spatial bins (tiles) of 100-µm width to assess lateral delays of adjacent tiles and vertical delays of tiles situated above each other. Right: population average calcium transients of individual tiles within LII/III or LV across all seizures in one experiment are shown (right, gray shades represent SEM, number of seizures = 11, number of analyzed cells = 102, number of spatial tiles = 8). Note that lateral but also vertical tile delays can be appreciated by eye.

(B) Boxplots of lateral (tile[prox] − tile[dist]) recruitment time lags of adjacent tiles within LII/III (left) or LV (right, n = 4 exp., total number of seizures = 32 [8 ± 3.6 SEM]). The boxes represent 25th–75th percentile, and the bands inside the boxes display the median recruitment time lag. In nearly all seizures, proximal tiles (lateral lag) were recruited prior to their adjacent distal tiles (for lateral lags LII/III and LV: chi-square test X2(1) = 12.7, $p < 0.001$). See also Figure S3D and Supplemental Experimental Procedures.

(C) Same 4 exp. as in (B). Boxplots of vertical recruitment time lags of adjacent tiles (tile[LII/III] − tile[LV]). In all seizures, LII/III tiles were recruited prior to their corresponding LV tiles (chi-square test X2(1) = 21.3, $p < 0.001$).

limb-related motor symptoms and, at times, alternatingly bilateral convulsions, occurred post local 4-AP or Ptx injection (Figures 5B and 5C). In spite of this, our local injection approach allowed for the study of spreading seizures under stable imaging conditions, since ictal recruitment of imaged cortical areas sufficiently often preceded seizure spread to motor cortices. In comparison to 4-AP, Ptx-induced seizures were generally short (4-AP: 71 ± 7.1 s [five exp., 26 seizures], Ptx: 19.1 ± 1.34 s [three exp., 19 seizures]). Additionally, Ptx injection commonly led to multitudes of IISs in the LFP, which, however, did not optically recruit the imaged FOV (Figure 5C). Interestingly, and consistently in awake mice, interictal periods and seizure durations displayed a rather irregular pattern. At times, ictal activity failed to invade or only incompletely penetrated the imaged territory (Figures 5B, left and 5C, left), and there was a consistent delay between the electrographic seizure onset and optical break-in on the scale of seconds (Figures 5B and 5C, magnified portions) (Khoshkhoo et al., 2017; Martinet et al., 2015). This observation could be explained by a much slower temporal seizure progression imaged during wakefulness as compared to the anesthetized condition (4-AP: 0.0215 ± 0.003 mm/s [five exp., awake] versus 0.64 ± 0.18 mm/s [seven exp., anesthetized]). Both the lack of optical penetration of IIS and the persistence of seconds of delay of optical break-in upon electrographic seizure onset present also in the Ptx model, over the duration of an entire experiment (Figure 5C, magnified portions), further supported that the injected chemoconvulsant remained local within the seizure initiation site and did not diffuse into the FOV.

During wakefulness, in line with our anesthetized recordings, neurons in the propagation area were recruited in a continuous, sigmoid temporal curve independently of the employed seizure model, yet over stretched time courses (Figure 5D; Movie S6). Cellular recruitment reliability to ictal activity persisted in awake mice, and it appeared to be even more pronounced than during anesthesia. In both 4-AP- and Ptx-induced seizures, we found a clear leftward shift of rr score SD distributions in the observed versus randomized data (Figure 5E), and, consequently, we obtained high cellular reliability indices, within and across layers (Figure 5F; 4-AP: five axial exp., one prism; Ptx: three exp.). Again, we excluded the possibility that these results were biased by the cells' indicator expression levels through a correlation analysis between cellular baseline fluorescence and the corresponding recruitment time (Figure S3E; transgenic GCaMP6f, five axial exp. [4-AP], 26 seizures, 360 cells, $r = 0.1675$, $r^2 = 0.0281$; the effect accounts for 2.8% of the variance in the data).

In agreement with our experiments in anesthetized mice, temporal population recruitment quartiles clustered into discriminable spatial domains (Figure 5G; 4-AP: 11 seizures, $F[3,40] = 18.44$, $p = 1.145 \times 10^{-7}$; Ptx: four seizures, $F[3,12] = 52.87$, $p = 1.591 \times 10^{-8}$; other 4-AP exp.: $F[3,12] = 138.48$, $F[3,8] = 15.89$, $F[3,12] = 32.19$, and $F[3,20] = 56.5$; other Ptx exp.: $F[3,20] = 447.98$ and $F[3,28] = 91.22$; all $p < 0.001$). Finally, layer-specific recruitment delays were also present in seizure spread during wakefulness. As described (Figure 4; Figure S3), we found significant layer-specific average negative time lags of proximal versus distal tiles in all seven seizures imaged through a microprism and consistent delays of local LV populations to their LII/III respective group of cells (Figure 5H). It is noteworthy that, while lateral time lags were prolonged during wakefulness, trans-laminar lags remained on par with the anesthetized condition. In conclusion, while differences in temporal seizure progression were found in awake versus anesthetized mice, relative ictal recruitment reliability of local neural networks, spatiotemporally ordered micro-progression, and layer-specific recruitment lags to spreading seizures were also present in experiments during wakefulness.

Seizure Micro-progression Is Elastic

While evaluating the spatiotemporal characteristics of local network recruitment by seizures in both the anesthetized and awake condition, we noticed that, despite the observed relative spatiotemporal stereotypy, the absolute ictal network recruitment varied profoundly in time. To further investigate this

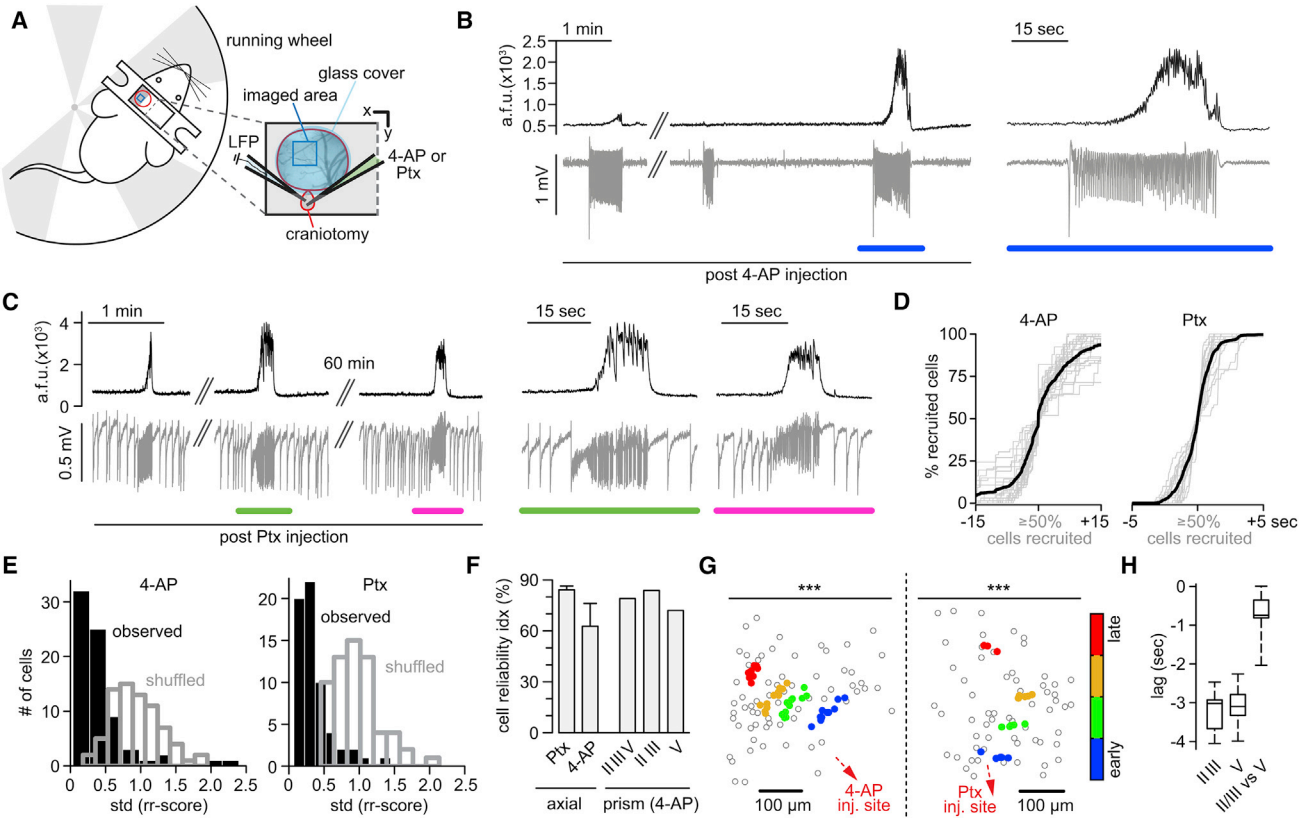

Figure 5. Stereotypical and Elastic Seizure Propagation in Awake Mice

(A) Adapted experimental setup (craniotomy outlined in red, FOV in dark blue, and glass coverslip in light blue). Two inserted glass pipettes were used (LFP [blue], 4-AP or Ptx [green, 4-AP: 500 nL, total amount delivered = 7.5 nmol; Ptx: 10 mM, 500 nL, total amount delivered = 5 nmol]).

(B) Average population calcium transient (black trace, Thy-1::GCaMP6f, LII/III) and corresponding LFP (gray trace) post 4-AP (~2 mm posterior to FOV in somatosensory cortex). Blue underscore marks magnified inset on the right.

(C) Average population calcium transient (black trace, Thy-1::GCaMP6f, LII/III) and corresponding LFP (gray trace) post Ptx (~1.5 mm posterior to FOV in somatosensory cortex). Green and magenta mark magnified insets on the right. Note the stable lack of calcium responses to IIS in the LFP and slow seizure invasion of the FOV post Ptx.

(D) Superposition of all axially imaged seizures (gray) in awake mice, post 4-AP or Ptx, centered around the 50% recruitment frame. The black graphs represent mean temporal recruitment (4-AP: n = 5 exp., total number of seizures = 26, total number of cells analyzed = 359 [72 ± 8 SEM]; Ptx: n = 3 exp., total number of seizures = 19, total number of cells analyzed = 182 [61 ± 1 SEM]; cell number in percentage for comparability across experiments).

(E) Representative experiment (4-AP or Ptx) with observed (black) versus shuffled (gray) rr score SD distributions. Both seizure models show leftward shifts of the observed versus shuffled data.

(F) Cellular reliability indices (rr score) across seizure models: Ptx (n = 3 exp., axial imaging) and 4-AP (n = 5 exp. axial imaging, n = 1 exp. multilayer imaging).

(G) Representative experiment (4-AP or Ptx). The spatial average coordinates of temporally defined population quartiles (colored dots) are plotted within the imaged population (gray circles represent individual cells); left: 4-AP (bivariate ANOVA: n = 11 seizures, $F[3,40] = 18.44$, $p = 1 \times 10^{-7}$, all five experiments in awake mice with 4-AP $p < 0.001$); right: Ptx (bivariate ANOVA: n = 4 seizures, $F[3,12] = 52.87$, $p = 1.5 \times 10^{-8}$, all three experiments in awake mice with Ptx $p < 0.001$).

(H) Multilayer imaging. Boxplots of lateral or vertical onset time lags of adjacent tiles are shown (please see also Figure S3D); boxes represent 25th–75th percentile, and bands inside boxes display the median recruitment time lag (n = 1 exp., 4-AP, total number of seizures = 7).

phenomenon, we defined the recruitment duration for each recorded seizure as the time period from the first to the last cell recruitment frame, excluding the 5% most deviant cells to the median recruitment frame to minimize outlier-related duration distortions. Across employed seizure models, population recruitment varied from hundreds of milliseconds to several seconds (Figure 6A). Strikingly, this variability was present within individual experiments too (Figure 6B; seven exp. [anesthesia], eight exp. [wakefulness]). Importantly, this phenomenon was not simply explained by a facilitating temporal compression over time, since successive seizures showed well-maintained relative spatiotemporal recruitment while their absolute time courses of recruitment compressed and stretched greatly (Figure S4A). While we could not find a systematic correlational relationship between electrographic seizure length and local population recruitment duration (Figure S4B), as has been previously described for macroscale ictal recruitment (Martinet et al., 2015), total seizure duration itself displayed temporal variability, too (Figure S4C). These results unveiled that neural recruitment to spreading seizures displays elastic features, that is, relative spatiotemporal reliability despite progression variability in absolute time.

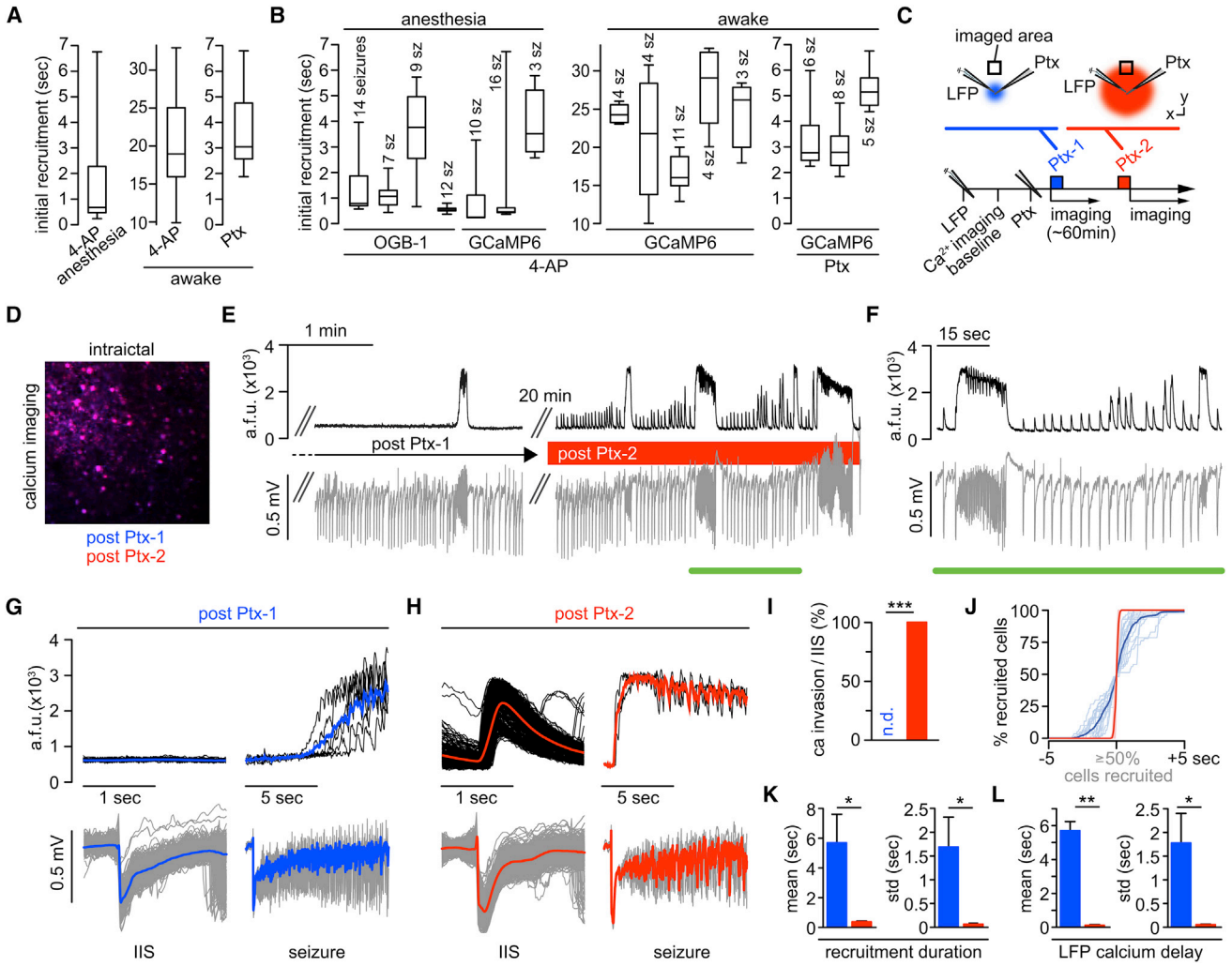

Figure 6. Elastic Recruitment Is Regulated by Local Inhibitory Neurons

(A) Absolute ictal recruitment durations vary across seizures. Boxplots display population recruitment durations analyzed for each condition; left: 4-AP under isoflurane (n = 7 exp., 71 seizures); middle: 4-AP during wakefulness (n = 5 exp., 26 seizures); right: Ptx during wakefulness (n = 3 exp., 19 seizures).

(B) Ictal recruitment durations vary within individual experiments. Boxplots of 15 exp. (n = 7 anesthesia and n = 8 wakefulness) are shown. Boxes represent 25th–75th percentile of cellular recruitment, and bands inside boxes display median cell recruitment time.

(C) Schematic depiction of experiments involving two Ptx injections during wakefulness: LFP and Ptx pipettes are located within the seizure initiation site. After LFP pipette insertion and baseline imaging, the Ptx (10-mM) pipette is inserted. The first Ptx injection (Ptx-1, blue) is volume controlled, as usual (500 nL, total amount delivered = 5 nmol]), and followed by imaging seizure spread, as described, for ~60 min. Then, a second Ptx injection (Ptx-2, red) is performed (pressure controlled, 10 psi, 10 min).

(D) Merged average images of ictal FOV post Ptx-1 (blue) and post Ptx-2 (red). Note the complete overlap of the average images (magenta); that is, the imaged focal plane remains stable beyond Ptx-2.

(E) Representative experiment; left: post Ptx-1, imaging (black) and LFP recordings (gray) of spreading seizures for >1 hr (note no calcium response to IIS in the LFP); right: ~20 min post Ptx-2.

(F) Magnification of inset in (E). Note that post Ptx-2, every IIS in the LFP coincides with a population calcium response within the FOV in the propagation area.

(G) Same experiment, post Ptx-1. Left: superimposed 2-s windows of population calcium activity are shown (top, individual traces in black, mean in blue), centered around 678 IISs recorded by LFP at the distant injection site (bottom, individual events in gray, mean in blue). Right: superimposed 10-s windows of six seizures recorded by imaging (top, individual seizures in black, mean in blue) and LFP (bottom, individual seizures in gray, mean in blue) are shown. Note the delay of several seconds between electrographic seizure onset and optical invasion.

(H) Same experiment, post Ptx-2. Left: superimposed 2-s windows of population calcium activity are shown (top, individual traces in black, mean in red), centered around 562 IISs (bottom, individual events in gray, mean in red). Right: superimposed 10-s windows of three seizures recorded by imaging (top, individual seizures in black, mean in red) and LFP (bottom, individual seizures in gray, mean in red) are shown. Note the clear population calcium response to IIS in the LFP and the immediate penetration of the imaged FOV upon electrographic seizure onset.

(I) Quantification of optical invasion per IIS (n = 4 exp., 1,327 IISs post Ptx-1 [n.d. = none detectable], 893 IISs post Ptx-2 [mean invasion rate = 100%]; Mann-Whitney test, p = 0).

(legend continued on next page)

Seizure Progression Elasticity Is Determined by Local Inhibition

To gain mechanistic insight into this phenomenon in vivo, we drew clues from previous work in acute brain slices, which provided evidence that interneuron activity governs the speed of ictal progression (Chagnac-Amitai and Connors, 1989; Trevelyan et al., 2007). To this end, we added a second part to the experiments involving local Ptx injection in awake mice. First, we injected Ptx (Ptx-1) and carried out imaging and LFP recordings as described. Then, after repeated seizure spread into our FOV under the usual condition, we pressure injected Ptx (Ptx-2) analogously to a typical OGB-1 injection (picrospritzer, ~10 psi for 10 min) (Ayzenshtat et al., 2016; Miller et al., 2014), at the same location where the first injection took place (Figure 6C). Post Ptx-2 injection, we were still able to image exactly the same FOV in the propagation area that was used post Ptx-1, without any distortion of the imaged plane (Figure 6D).

When we resumed imaging and LFP recordings post Ptx-2, we found profoundly different local population dynamics in response to IISs and during seizures (Figure 6E). Prior to Ptx-2, IISs did not coincide with optical population responses in the FOV, and optical seizure break-in happened slowly (Figures 5C, 6A, right, 6E, left, and 6G). Post Ptx-2, we started to see reliable calcium responses to IISs and rapid seizure invasion (Figures 6E, right, 6F, and 6H), suggesting that Ptx had diffused to the imaged territory. In fact, prior to complete drug diffusion across our FOV, it was possible to identify a demarcation line between tissue that had already been affected by the drug and tissue where inhibition was still intact (Figure S4D). While cells being located proximally to the said demarcation line rapidly responded to IISs, brief and prolonged ictal events, distally located cells were recruited only to prolonged seizures, in a delayed fashion and at much lower speed (Figure S4D). Importantly, the trajectory of seizure propagation across the FOV remained similar to the condition prior to Ptx-2 (compare Figures S4A, bottom and S4D).

To quantify differences in interictal and ictal network recruitment dynamics related to Ptx-1 or Ptx-2 across animals, we compared population calcium responses to electrographic IISs (recorded at the initiation site), the time delay between electrographic seizure onset and optical seizure break-in, and the local population recruitment. Indeed, post Ptx-1, IISs were never followed by a change in local population calcium, while after Ptx-2, IISs consistently evoked a response (Figure 6I; calcium response rate per IIS [Ptx-1 versus Ptx-2]: n = 4 exp., 1,327 versus 893 IISs, 0% versus 100% invasion rate, p = 0). With respect to spreading seizures, the imaged population was recruited slowly and with great temporal variability post Ptx-1, while both ictal recruitment duration and duration SD decreased strongly post Ptx-2 (Figures 6J and 6K; [Ptx-1 versus Ptx-2]: n = 4 exp., mean recruitment duration 5.696 ± 1.915 versus 0.375 ± 0.052 s, p = 0.0286; mean recruitment duration SD 1.69 ± 0.625 versus 0.068 ± 0.024 s, p = 0.0286). Similar results were obtained for the time delay between the electrographic seizure onset and optical seizure break-in (Figure 6L; [Ptx-1 versus Ptx-2]: n = 4 exp., mean delay 5.7 ± 0.538 versus 0.116 ± 0.038 s, p = 0.002; mean delay SD 1.78 ± 0.62 versus 0.055 ± 0.012 s, p = 0.0286). In conjunction with our cellular recruitment analyses, these experiments revealed that elasticity and speed of microscale seizure progression critically depends on the activity of local inhibitory interneurons.

DISCUSSION

Stereotypical Propagation of Epileptic Seizures in Cortical Microcircuits

Partly due to a lack of studies with appropriate temporal and spatial resolution, an ongoing debate has remained as to whether or not the recruitment of microscale networks to ictal activity happens in a stereotypical or random fashion. To address this question, we combined LFP recordings with fast resonant two-photon calcium imaging in mouse models of locally induced acute seizures, finding robust stereotypical and reliable recruitment. Our findings hold true across anesthesia and wakefulness, two different seizure models (4-AP or Ptx), and cortical areas. Most experiments in this study involved imaging of somatosensory cortex (LII/III) after local 4-AP or Ptx injection at 1.5–3 mm posterior to the FOV. However, we also performed experiments where we imaged in visual cortex with the injection site being located anterior, with consistent results (Figure S5). This suggests that, at the least in the setting of acute seizures, our results (1) reflect basic patterns of ictal spread, (2) are independent of the experimental model of focal onset seizures, and (3) apply across cortical areas.

Our experiments support previous work on the existence of ictal network stereotypy (Schevon et al., 2012; Truccolo et al., 2011), yet they show that local network reliability is not exact. This is consistent with previous studies that show that, under normal conditions, cortical microcircuits generate repeated patterns of multicellular activity that are, however, never exact (Cossart et al., 2003; Ikegaya et al., 2004; Miller et al., 2014). In addition, by use of multilayer imaging, we show that cellular recruitment reliability to spreading seizures is not restricted to LII/III but holds true across cortical depth. Our results do not support reports of fully non-repeated ictal recruitment patterns (Bower et al., 2012), and they further suggest that the observation of unpredictable spatiotemporal recruitment of local cell assemblies to seemingly stereotypical interictal spikes in the LFP

(J) Superposition of all optical invasions during electrographic seizures (n = 4 exp.; post Ptx-1: 21 seizures, individual events in light blue, mean in dark blue; post Ptx-2: 17 seizures, individual events in light red, mean in dark red), centered around the 50% recruitment frame of the population (cell number in percentage for comparability across experiments). Note how the slow, s-curved population recruitment curve upon Ptx-1 changes into a near step-like function post Ptx-2.

(K) Quantitative comparison of absolute population recruitment duration and duration SD of the Ptx-1 (blue) versus Ptx-2 (red) condition (n = 4 exp., Ptx-1/Ptx-2: 21/17 seizures): mean recruitment duration (5.696 ± 1.915 versus 0.375 ± 0.052 s; Mann-Whitney test, p = 0.0286) and mean recruitment duration SD (1.69 ± 0.625 versus 0.068 ± 0.024 s, p = 0.0286).

(L) Quantitative comparison of absolute time delay and delay SD of optical invasion after electrographic seizure onset of the Ptx-1 (blue) versus Ptx-2 (red) condition (n = 4 exp., Ptx-1/Ptx-2: 21/17 seizures): mean delay (5.7 ± 0.538 versus 0.116 ± 0.038 s; Mann-Whitney test, p = 0.002) and mean delay SD (1.78 ± 0.62 versus 0.055 ± 0.012 s, p = 0.0286).

(Feldt Muldoon et al., 2013; Muldoon et al., 2015) may not apply to the local recruitment dynamics during cortical seizure spread. In line with previous cellular resolution imaging studies in slices during interictal and ictal conditions (Badea et al., 2001; Feldt Muldoon et al., 2013; Trevelyan et al., 2006) and reports employing wide-field imaging (Ma et al., 2013; Rossi et al., 2016), we show that ictal recruitment of local networks occurs in a spatially ordered manner.

Interlaminar Stereotypical Propagation of Epileptic Seizures

There is evidence that deep cortical layers are crucially involved in focal ictogenesis, where they precede the recruitment of superficial neurons to ictal activity (Connors, 1984; Polack et al., 2007; Rheims et al., 2008; Telfeian and Connors, 1998; Trevelyan et al., 2006; but see also Tsau et al., 1999). However, the layer-specific neural dynamics during lateral seizure spread have not been extensively studied (Adams et al., 2015; Borbély et al., 2006; Telfeian and Connors, 1998; Tsau et al., 1999), and exclusively in vitro. Our results show an initial recruitment of superficial layers during lateral spread of ictal activity, which seems in contrast to a previous study in brain slices where deep layers were observed to lead lateral seizure spread when inhibition was moderately reduced (Telfeian and Connors, 1998). Under such conditions, seizure propagation was dependent on intact tissue bridges within LIV to LVI, and it was most effectively blocked when LVb was inactivated by local GABA administration. However, the same study showed that, under high doses of Ptx, lateral seizure propagation was possible in each layer separately.

Considering the experimental restrictions of both our study and Telfeian and Connor's report, several factors could account for the seemingly discrepant results. First, there is the inherently impaired neural connectivity in acute brain slices, which could have influenced the previously reported findings. Even though prism insertion in our experiments is expected to have affected cortical connectivity in the vicinity of the imaged FOV as well, it did so to a lesser extent, leaving most of the anatomical and functional cortical and subcortical connections intact. Second, bath application of disinhibitory drugs to brain slices leads to a global impairment of inhibition, which is unlikely to take place similarly in the intact brain. While our data point away from LV and favor LII/III as the lead layer during lateral ictal spread, it remains possible that this spread could in fact be led by LIV. This layer was consistently nearly devoid of labeled cells in our study (this has been observed in other studies as well, and cannot only be explained by injection depth; Andermann et al., 2013; Chia and Levene, 2009a). In this case, LIV neurons could suppress LV and activate superficial layers, which subsequently signal to LV (Thomson and Bannister, 2003), a scenario convergent with known connectivity motifs in mouse somatosensory cortex (Pluta et al., 2015). Our findings bear potential implications for neurosurgical intervention in epilepsy, as they indicate (e.g., regarding sub-pial resections) that the disconnection of LII/III alone could be sufficient to stop lateral seizure spread.

Clinical Relevance

This study concentrated on basic aspects of seizure spread into cortical areas that surround an acutely established epileptic focus. We capitalized on aspects that are shared between our approach and medical conditions such as brain trauma, which often present with acute seizures without the process of epileptogenesis (Beleza, 2012). Our results also carry potential implications for chronic epilepsies with focal onset seizures. There, territories outside the epileptic focus remain functionally intact, and thus they resemble the local networks imaged in this study. Instead of focusing on a specific disease pathway, we rather considered seizures as a phenomenon shared by many neurological disorders and even the healthy brain (Jirsa et al., 2014). Further, the approach of local injection of 4-AP or Ptx represents widely established models of partial onset seizures eliciting electrographic phenomena and behavioral symptoms that resemble those in naturally occurring epilepsy (Avoli et al., 2002; Szente and Pongrácz, 1979) and have contributed successfully to therapeutic research (Gajda et al., 2005; Rothman, 2009). The total amount of injected 4-AP or Ptx was small (7.5 or 5 nmol, respectively). The fact that we did not see enhanced firing in the imaged region prior to seizure break-in, neither post 4-AP nor Ptx (Ptx-1), and that particularly after local Ptx injection no change in local calcium activity was observed in response to IISs in the LFP, over the entire experiment, underscores that we imaged within the propagation area and make it unlikely that the imaged area was directly exposed to 4-AP or Ptx. Only after prolonged pressure injection of Ptx (Ptx-2) did we see a change in local calcium dynamics toward typical network activity manifestations induced by Ptx, which suggested that the drug had finally diffused to the imaged FOV.

We did not image the dynamics of precisely defined neural sub-populations during seizures. There is evidence, including the data presented here, that the local interaction of excitatory and inhibitory circuits is crucial for successful or failed ictal progression (Cammarota et al., 2013; Hunt et al., 2013; Khoshkhoo et al., 2017; Sessolo et al., 2015; Trevelyan et al., 2006; Ziburkus et al., 2006). While several recent studies have shown promising results with respect to cell sub-population-based therapeutic seizure intervention (Krook-Magnuson et al., 2013; Ledri et al., 2014), others have raised concerns about the potential seizure-promoting effects of such therapies (Avoli and de Curtis, 2011; Fujiwara-Tsukamoto et al., 2010; Gnatkovsky et al., 2008; Grasse et al., 2013; Sessolo et al., 2015). This controversy highlights that our knowledge of the basic dynamics of densely packed local ictal networks and the neural sub-types therein has remained unsatisfying. Future studies applying fast high-density recordings of neural networks and sub-populations during seizures will be important in substantiating our understanding of epileptic networks and identifying novel therapeutic targets for more efficient seizure control.

Elastic Cortical Seizure Propagation and Its Potential Relevance for Cortical Function

Finally, despite a repeated relative spatiotemporal structure of seizure progression, we found variable absolute temporal recruitment of local cell populations within and across experiments. This elastic progression, which could stretch in time over seconds, could be interpreted in light of Hebb's phase sequences (Hebb, 1949) or sequential activation of local cell assemblies and other intrinsic network dynamics (Harris, 2005)

that shape temporal activity patterns of neural cell populations (Carrillo-Reid et al., 2015; Cossart et al., 2003; Harris, 2005; Ikegaya et al., 2004; Luczak et al., 2013; MacLean et al., 2005; Schölvinck et al., 2015; Skaggs et al., 1996). Based on this model, an expanding seizure could constitute the extreme version of a phase sequence whose temporal properties are governed by *local* internal dynamics, such as the level of sustained synaptic input or efficacy of inhibition, and *global* internal dynamics, like state of arousal or global network synchrony. Testable factors likely affecting these dynamics with respect to seizures could, for example, involve the distance from the seizure initiation site, age or gender of the studied subject, different oscillatory brain states (Ewell et al., 2015), or differentially evoked firing patterns of distinct interneuronal sub-populations (Adesnik et al., 2012). Indeed, there is evidence, for example, that velocity of ictal expansion depends on the activity of inhibitory interneurons (Prince and Wilder, 1967; Trevelyan et al., 2007). We substantiate this evidence in vivo by showing that local compromising of GABAergic signaling results in the abolishment of ictal micro-progression elasticity and a speed-up of local seizure spread. However, the preexistent anatomical framework of specifically interconnected neurons restrains the possibilities of spatial seizure progression within the network.

Altogether, our finding of substantial temporal variability in combination with considerable relative spatiotemporal reliability of dense local networks during successive seizures suggests a network model of epilepsy resembling an elastic meshwork, wherein ictal progression may vary in time but cannot betray preexistent neural connectivity. Our results also carry potential implications for physiological cortical processing, and they are in agreement with previous studies investigating sequential ensemble activation (Ikegaya et al., 2004; Luczak et al., 2013; MacLean et al., 2005; Malvache et al., 2016; Schölvinck et al., 2015; Skaggs et al., 1996). Far from clock-driven machines, such as digital computers, it is fascinating to speculate how cortical circuits could function by activating specific dynamical trajectories that could be engaged elastically at different timescales. This flexible temporal environment could enable sensory stimuli to be integrated even if they have temporal variability, make possible for different areas of the cortex to interact in a flexible manner, and perhaps also influence an individual's decision-making depending on the differential temporal convergence of sensory information.

EXPERIMENTAL PROCEDURES

Further details and an outline of resources used in this work can be found in the Supplemental Experimental Procedures. All experiments were conducted with care and in accordance with the Columbia University institutional animal care guidelines. Experiments were carried out on C57BL/6 adult mice at post-natal age of 1–3 months. LFP measurements and concomitant in vivo two-photon calcium imaging were performed 1 hr after cortical Oregon Bapta Green-1 AM injection, 4–5 weeks after lentiviral transfer of GCaMP6s, or in transgenic Thy1-GCaMP6f animals. For experiments involving multilayer imaging, a small glass microprism was implanted into the cortex. A part of the craniotomy remained uncovered in front of the prism face to allow access for the LFP and 4-AP micropipettes. Seizure induction was achieved through local injection of small amounts of either 4-AP or Ptx into LV. The distance between the seizure initiation site and the imaged area ranged from 1.5 to 3 mm. Cell regions of interest (ROIs) were identified in a semi-automated fashion followed by manual confirmation. To identify the ictal recruitment time point of individual cells, we used the first discrete derivative (slope) of the ΔF/F traces following electrographic seizure onset. For assessment of individual cell recruitment reliability, a time bin or relative recruitment score (rr score) classification was used and compared to a shuffled surrogate. All data were analyzed using custom-written code in MATLAB. Error bars on bar plots and shaded areas in graph plots indicate SEM. Reliability indices of cells or tiles were compared using one-way ANOVA. Spatiotemporal clustering was assessed by bivariate ANOVA of mean distance differences. In multilayer-imaging experiments, spatial tile onset order distributions were compared to an even distribution (16 proximal/16 distal and 16 superficial/16 deep) with a 2 × 2 chi-square test. With respect to optical seizure invasion rate, cellular recruitment durations, duration SD, LFP to calcium delays, and delay SD, two experimental groups (Ptx-1 versus Ptx-2; Figures 6I, 6K, and 6L) were compared across experiments by Mann-Whitney test.

SUPPLEMENTAL INFORMATION

Supplemental Information includes Supplemental Experimental Procedures, five figures, and six movies and can be found with this article online at http://dx.doi.org/10.1016/j.celrep.2017.05.090.

AUTHOR CONTRIBUTIONS

M.W. and R.Y. conceived of the project. M.W. performed all experiments and wrote the paper. M.W. and J.P.H. analyzed the data. All authors planned experiments, discussed results, and edited the paper.

ACKNOWLEDGMENTS

We thank Dr. Yeonsook Shin and Alexa Semonche for viral injections and to members of the Yuste, Schwartz, and Schevon laboratories for comments. This work was supported by the Deutsche Forschungsgemeinschaft (DFG, grant WE 5517/1-1), NEI (DP1EY024503 and R01EY011787), NIMH (R01MH101218 and R01MH100561), and DARPA SIMPLEX N66001-15-C-4032. This material is based on work supported by, or in part by, the U.S. Army Research Laboratory and the U.S. Army Research Office under contract number W911NF-12-1-0594 (MURI).

Received: July 27, 2016
Revised: May 15, 2017
Accepted: May 28, 2017
Published: June 27, 2017

REFERENCES

Adams, C., Adams, N.E., Traub, R.D., and Whittington, M.A. (2015). Electrographic waveform structure predicts laminar focus location in a model of temporal lobe seizures in vitro. PLoS ONE *10*, e0121676.

Adesnik, H., Bruns, W., Taniguchi, H., Huang, Z.J., and Scanziani, M. (2012). A neural circuit for spatial summation in visual cortex. Nature *490*, 226–231.

Andermann, M.L., Gilfoy, N.B., Goldey, G.J., Sachdev, R.N., Wölfel, M., McCormick, D.A., Reid, R.C., and Levene, M.J. (2013). Chronic cellular imaging of entire cortical columns in awake mice using microprisms. Neuron *80*, 900–913.

Avoli, M., and de Curtis, M. (2011). GABAergic synchronization in the limbic system and its role in the generation of epileptiform activity. Prog. Neurobiol. *95*, 104–132.

Avoli, M., D'Antuono, M., Louvel, J., Köhling, R., Biagini, G., Pumain, R., D'Arcangelo, G., and Tancredi, V. (2002). Network and pharmacological mechanisms leading to epileptiform synchronization in the limbic system in vitro. Prog. Neurobiol. *68*, 167–207.

Ayzenshtat, I., Karnani, M.M., Jackson, J., and Yuste, R. (2016). Cortical Control of Spatial Resolution by VIP+ Interneurons. J. Neurosci. *36*, 11498–11509.

Badea, T., Goldberg, J., Mao, B., and Yuste, R. (2001). Calcium imaging of epileptiform events with single-cell resolution. J. Neurobiol. *48*, 215–227.

Baird-Daniel, E., Daniel, A.G., Wenzel, M., Li, D., Liou, J.Y., Laffont, P., Zhao, M., Yuste, R., Ma, H., and Schwartz, T.H. (2017). Glial Calcium Waves are Triggered by Seizure Activity and Not Essential for Initiating Ictal Onset or Neurovascular Coupling. Cereb. Cortex *27*, 3318–3330.

Baraban, S.C., and Löscher, W. (2014). What new modeling approaches will help us identify promising drug treatments? Adv. Exp. Med. Biol. *813*, 283–294.

Beleza, P. (2012). Acute symptomatic seizures: a clinically oriented review. Neurologist *18*, 109–119.

Borbély, S., Halasy, K., Somogyvári, Z., Détári, L., and Világi, I. (2006). Laminar analysis of initiation and spread of epileptiform discharges in three in vitro models. Brain Res. Bull. *69*, 161–167.

Bower, M.R., Stead, M., Meyer, F.B., Marsh, W.R., and Worrell, G.A. (2012). Spatiotemporal neuronal correlates of seizure generation in focal epilepsy. Epilepsia *53*, 807–816.

Cammarota, M., Losi, G., Chiavegato, A., Zonta, M., and Carmignoto, G. (2013). Fast spiking interneuron control of seizure propagation in a cortical slice model of focal epilepsy. J. Physiol. *591*, 807–822.

Carrillo-Reid, L., Miller, J.-E.K., Hamm, J.P., Jackson, J., and Yuste, R. (2015). Endogenous sequential cortical activity evoked by visual stimuli. J. Neurosci. *35*, 8813–8828.

Chagnac-Amitai, Y., and Connors, B.W. (1989). Horizontal spread of synchronized activity in neocortex and its control by GABA-mediated inhibition. J. Neurophysiol. *61*, 747–758.

Chen, T.W., Wardill, T.J., Sun, Y., Pulver, S.R., Renninger, S.L., Baohan, A., Schreiter, E.R., Kerr, R.A., Orger, M.B., Jayaraman, V., et al. (2013). Ultrasensitive fluorescent proteins for imaging neuronal activity. Nature *499*, 295–300.

Chia, T.H., and Levene, M.J. (2009a). In vivo imaging of deep cortical layers using a microprism. J. Vis. Exp. (*30*), 1509.

Chia, T.H., and Levene, M.J. (2009b). Microprisms for in vivo multilayer cortical imaging. J. Neurophysiol. *102*, 1310–1314.

Connors, B.W. (1984). Initiation of synchronized neuronal bursting in neocortex. Nature *310*, 685–687.

Cossart, R., Aronov, D., and Yuste, R. (2003). Attractor dynamics of network UP states in the neocortex. Nature *423*, 283–288.

Cymerblit-Sabba, A., and Schiller, Y. (2012). Development of hypersynchrony in the cortical network during chemoconvulsant-induced epileptic seizures in vivo. J. Neurophysiol. *107*, 1718–1730.

Ewell, L.A., Liang, L., Armstrong, C., Soltész, I., Leutgeb, S., and Leutgeb, J.K. (2015). Brain State Is a Major Factor in Preseizure Hippocampal Network Activity and Influences Success of Seizure Intervention. J. Neurosci. *35*, 15635–15648.

Feldt Muldoon, S., Soltesz, I., and Cossart, R. (2013). Spatially clustered neuronal assemblies comprise the microstructure of synchrony in chronically epileptic networks. Proc. Natl. Acad. Sci. USA *110*, 3567–3572.

Fujiwara-Tsukamoto, Y., Isomura, Y., Imanishi, M., Ninomiya, T., Tsukada, M., Yanagawa, Y., Fukai, T., and Takada, M. (2010). Prototypic seizure activity driven by mature hippocampal fast-spiking interneurons. J. Neurosci. *30*, 13679–13689.

Gajda, Z., Szupera, Z., Blazsó, G., and Szente, M. (2005). Quinine, a blocker of neuronal cx36 channels, suppresses seizure activity in rat neocortex in vivo. Epilepsia *46*, 1581–1591.

Gnatkovsky, V., Librizzi, L., Trombin, F., and de Curtis, M. (2008). Fast activity at seizure onset is mediated by inhibitory circuits in the entorhinal cortex in vitro. Ann. Neurol. *64*, 674–686.

Grasse, D.W., Karunakaran, S., and Moxon, K.A. (2013). Neuronal synchrony and the transition to spontaneous seizures. Exp. Neurol. *248*, 72–84.

Harris, K.D. (2005). Neural signatures of cell assembly organization. Nat. Rev. Neurosci. *6*, 399–407.

Hebb, D.O. (1949). The Organization of Behavior (New York: Wiley).

Hunt, R.F., Girskis, K.M., Rubenstein, J.L., Alvarez-Buylla, A., and Baraban, S.C. (2013). GABA progenitors grafted into the adult epileptic brain control seizures and abnormal behavior. Nat. Neurosci. *16*, 692–697.

Ikegaya, Y., Aaron, G., Cossart, R., Aronov, D., Lampl, I., Ferster, D., and Yuste, R. (2004). Synfire chains and cortical songs: temporal modules of cortical activity. Science *304*, 559–564.

Jasper, H.H. (1969). Mechanisms of propagation: extracellular studies. In Basic mechanisms of the epilepsies, H.H. Jasper, A.A. Ward, and A. Pope, eds. (New York: Little, Brown).

Jirsa, V.K., Stacey, W.C., Quilichini, P.P., Ivanov, A.I., and Bernard, C. (2014). On the nature of seizure dynamics. Brain *137*, 2210–2230.

Keller, C.J., Truccolo, W., Gale, J.T., Eskandar, E., Thesen, T., Carlson, C., Devinsky, O., Kuzniecky, R., Doyle, W.K., Madsen, J.R., et al. (2010). Heterogeneous neuronal firing patterns during interictal epileptiform discharges in the human cortex. Brain *133*, 1668–1681.

Khoshkhoo, S., Vogt, D., and Sohal, V.S. (2017). Dynamic, Cell-Type-Specific Roles for GABAergic Interneurons in a Mouse Model of Optogenetically Inducible Seizures. Neuron *93*, 291–298.

Krishek, B.J., Moss, S.J., and Smart, T.G. (1996). A functional comparison of the antagonists bicuculline and picrotoxin at recombinant GABAA receptors. Neuropharmacology *35*, 1289–1298.

Krook-Magnuson, E., and Soltesz, I. (2015). Beyond the hammer and the scalpel: selective circuit control for the epilepsies. Nat. Neurosci. *18*, 331–338.

Krook-Magnuson, E., Armstrong, C., Oijala, M., and Soltesz, I. (2013). On-demand optogenetic control of spontaneous seizures in temporal lobe epilepsy. Nat. Commun. *4*, 1376.

Ledri, M., Madsen, M.G., Nikitidou, L., Kirik, D., and Kokaia, M. (2014). Global optogenetic activation of inhibitory interneurons during epileptiform activity. J. Neurosci. *34*, 3364–3377.

Lillis, K.P., Wang, Z., Mail, M., Zhao, G.Q., Berdichevsky, Y., Bacskai, B., and Staley, K.J. (2015). Evolution of Network Synchronization during Early Epileptogenesis Parallels Synaptic Circuit Alterations. J. Neurosci. *35*, 9920–9934.

Luczak, A., Bartho, P., and Harris, K.D. (2013). Gating of sensory input by spontaneous cortical activity. J. Neurosci. *33*, 1684–1695.

Ma, H., Zhao, M., and Schwartz, T.H. (2013). Dynamic neurovascular coupling and uncoupling during ictal onset, propagation, and termination revealed by simultaneous in vivo optical imaging of neural activity and local blood volume. Cereb. Cortex *23*, 885–899.

MacLean, J.N., Watson, B.O., Aaron, G.B., and Yuste, R. (2005). Internal dynamics determine the cortical response to thalamic stimulation. Neuron *48*, 811–823.

Malvache, A., Reichinnek, S., Villette, V., Haimerl, C., and Cossart, R. (2016). Awake hippocampal reactivations project onto orthogonal neuronal assemblies. Science *353*, 1280–1283.

Martinet, L.E., Ahmed, O.J., Lepage, K.Q., Cash, S.S., and Kramer, M.A. (2015). Slow Spatial Recruitment of Neocortex during Secondarily Generalized Seizures and Its Relation to Surgical Outcome. J. Neurosci. *35*, 9477–9490.

Miller, J.E., Ayzenshtat, I., Carrillo-Reid, L., and Yuste, R. (2014). Visual stimuli recruit intrinsically generated cortical ensembles. Proc. Natl. Acad. Sci. USA *111*, E4053–E4061.

Morales-Villagrán, A., and Tapia, R. (1996). Preferential stimulation of glutamate release by 4-aminopyridine in rat striatum in vivo. Neurochem. Int. *28*, 35–40.

Muldoon, S.F., Villette, V., Tressard, T., Malvache, A., Reichinnek, S., Bartolomei, F., and Cossart, R. (2015). GABAergic inhibition shapes interictal dynamics in awake epileptic mice. Brain *138*, 2875–2890.

Neubauer, F.B., Sederberg, A., and MacLean, J.N. (2014). Local changes in neocortical circuit dynamics coincide with the spread of seizures to thalamus in a model of epilepsy. Front. Neural Circuits *8*, 101.

Pluta, S., Naka, A., Veit, J., Telian, G., Yao, L., Hakim, R., Taylor, D., and Adesnik, H. (2015). A direct translaminar inhibitory circuit tunes cortical output. Nat. Neurosci. *18*, 1631–1640.

Polack, P.O., Guillemain, I., Hu, E., Deransart, C., Depaulis, A., and Charpier, S. (2007). Deep layer somatosensory cortical neurons initiate spike-and-wave discharges in a genetic model of absence seizures. J. Neurosci. *27*, 6590–6599.

Prince, D.A., and Wilder, B.J. (1967). Control mechanisms in cortical epileptogenic foci. "Surround" inhibition. Arch. Neurol. *16*, 194–202.

Rheims, S., Represa, A., Ben-Ari, Y., and Zilberter, Y. (2008). Layer-specific generation and propagation of seizures in slices of developing neocortex: role of excitatory GABAergic synapses. J. Neurophysiol. *100*, 620–628.

Rossi, L.F., Wykes, R.C., Kullman, D., and Carandini, M. (2016). Cortical seizure propagation respects functional connectivity underlying sensory processing. bioRxiv. http://dx.doi.org/10.1101/080598.

Rothman, S.M. (2009). The therapeutic potential of focal cooling for neocortical epilepsy. Neurotherapeutics *6*, 251–257.

Schevon, C.A., Weiss, S.A., McKhann, G., Jr., Goodman, R.R., Yuste, R., Emerson, R.G., and Trevelyan, A.J. (2012). Evidence of an inhibitory restraint of seizure activity in humans. Nat. Commun. *3*, 1060.

Schölvinck, M.L., Saleem, A.B., Benucci, A., Harris, K.D., and Carandini, M. (2015). Cortical state determines global variability and correlations in visual cortex. J. Neurosci. *35*, 170–178.

Sessolo, M., Marcon, I., Bovetti, S., Losi, G., Cammarota, M., Ratto, G.M., Fellin, T., and Carmignoto, G. (2015). Parvalbumin-Positive Inhibitory Interneurons Oppose Propagation But Favor Generation of Focal Epileptiform Activity. J. Neurosci. *35*, 9544–9557.

Skaggs, W.E., McNaughton, B.L., Wilson, M.A., and Barnes, C.A. (1996). Theta phase precession in hippocampal neuronal populations and the compression of temporal sequences. Hippocampus *6*, 149–172.

Stosiek, C., Garaschuk, O., Holthoff, K., and Konnerth, A. (2003). In vivo two-photon calcium imaging of neuronal networks. Proc. Natl. Acad. Sci. USA *100*, 7319–7324.

Szabo, G.G., Schneider, C.J., and Soltesz, I. (2015). Resolution revolution: epilepsy dynamics at the microscale. Curr. Opin. Neurobiol. *31*, 239–243.

Szente, M., and Pongrácz, F. (1979). Aminopyridine-induced seizure activity. Electroencephalogr. Clin. Neurophysiol. *46*, 605–608.

Tashiro, A., Goldberg, J., and Yuste, R. (2002). Calcium oscillations in neocortical astrocytes under epileptiform conditions. J. Neurobiol. *50*, 45–55.

Telfeian, A.E., and Connors, B.W. (1998). Layer-specific pathways for the horizontal propagation of epileptiform discharges in neocortex. Epilepsia *39*, 700–708.

Thomson, A.M., and Bannister, A.P. (2003). Interlaminar connections in the neocortex. Cereb. Cortex *13*, 5–14.

Trevelyan, A.J., Sussillo, D., Watson, B.O., and Yuste, R. (2006). Modular propagation of epileptiform activity: evidence for an inhibitory veto in neocortex. J. Neurosci. *26*, 12447–12455.

Trevelyan, A.J., Sussillo, D., and Yuste, R. (2007). Feedforward inhibition contributes to the control of epileptiform propagation speed. J. Neurosci. *27*, 3383–3387.

Truccolo, W., Donoghue, J.A., Hochberg, L.R., Eskandar, E.N., Madsen, J.R., Anderson, W.S., Brown, E.N., Halgren, E., and Cash, S.S. (2011). Single-neuron dynamics in human focal epilepsy. Nat. Neurosci. *14*, 635–641.

Truccolo, W., Ahmed, O.J., Harrison, M.T., Eskandar, E.N., Cosgrove, G.R., Madsen, J.R., Blum, A.S., Potter, N.S., Hochberg, L.R., and Cash, S.S. (2014). Neuronal ensemble synchrony during human focal seizures. J. Neurosci. *34*, 9927–9944.

Tsau, Y., Guan, L., and Wu, J.Y. (1999). Epileptiform activity can be initiated in various neocortical layers: an optical imaging study. J. Neurophysiol. *82*, 1965–1973.

Wong, B.Y., and Prince, D.A. (1990). The lateral spread of ictal discharges in neocortical brain slices. Epilepsy Res. *7*, 29–39.

Yuste, R., and Denk, W. (1995). Dendritic spines as basic functional units of neuronal integration. Nature *375*, 682–684.

Yuste, R., and Katz, L.C. (1991). Control of postsynaptic Ca2+ influx in developing neocortex by excitatory and inhibitory neurotransmitters. Neuron *6*, 333–344.

Ziburkus, J., Cressman, J.R., Barreto, E., and Schiff, S.J. (2006). Interneuron and pyramidal cell interplay during in vitro seizure-like events. J. Neurophysiol. *95*, 3948–3954.